Fu, Y., van Berk, W., Schulz, H.-M., Mu, N. (2015): Berthierine formation in reservoir rocks from the Siri oilfield (Danish North Sea) as result of fluid-rock interactions: Part II. Deciphering organic-inorganic processes by hydrogeochemical modeling. - *Marine and Petroleum Geology*, *65*, p. 317-326.

DOI: http://doi.org/10.1016/j.marpetgeo.2015.01.007

Marine and Petroleum Geology 65 (2015) 317–326

Contents lists available at ScienceDirect

Marine and Petroleum Geology

journal homepage: www.elsevier.com/locate/marpetgeo

Research paper

Berthierine formation in reservoir rocks from the Siri oilfield (Danish North Sea) as result of fluid–rock interactions: Part II. Deciphering organic–inorganic processes by hydrogeochemical modeling

Yunjiao Fu [a, 1], Wolfgang van Berk [b, *], Hans-Martin Schulz [a], Nana Mu [a]

[a] Helmhotz Centre Potsdam–GFZ German Research Centre for Geosciences, Section 4.3 Organic Geochemistry, Telegrafenberg, D-14473 Potsdam, Germany
[b] Clausthal University of Technology, Department of Hydrogeology, Leibnizstraße 10, D-38678 Clausthal-Zellerfeld, Germany

ARTICLE INFO

Article history:
Received 4 July 2014
Received in revised form
7 January 2015
Accepted 15 January 2015
Available online 30 January 2015

Keywords:
Berthierine
Glauconite
Hydrocarbon–water–rock–gas interactions
Hydrogeochemical modeling
Siri oilfield
Danish North Sea

ABSTRACT

Berthierine formation reduces the permeability of the glauconitic reservoir sandstones in the Siri oilfield (Danish North Sea), and is therefore a considerable production factor. A new hydrogeochemical batch model that is based on thermodynamics of chemical equilibrium was developed to identify the processes which activated and controlled berthierine formation. A good match has been achieved between the mineralogical alteration features observed in the Siri field and the results of the batch modeling. This match points to the validity of the modeling mechanisms for berthierine formation. Based on the identified mechanisms, the modeling enables to quantify the mass conversion of hydrogeochemical processes in glauconite-bearing and berthierine-forming water–rock–gas systems. The modeling results reveal that intense berthierine formation in the Siri field resulted from *in situ* glauconite alteration within a more or less closed system due to hydrocarbon degradation-driven water–rock–gas interactions. This process is accompanied by formation of secondary $SiO_{2(s)}$ and potassium mica. Precipitation of iron-bearing carbonates is prevented by berthierine formation, although the glauconitic sandstones are rich in iron and carbonate species. Moreover, such systems are brought to disequilibrium by the release of reducing and acidic agents originating from oil degradation, and undergo long-term, diffusion-dominated mass fluxes instead of advective mass fluxes.

1. Introduction and aim

Berthierine ($(Fe^{2+},Mg,Al)_{2-3}(Si,Al)_2O_5(OH)_4$), a dark green to brown mineral (Hornibrook and Longstaffe, 1996), commonly occurs in marine sediments (Iijima and Matsumoto, 1982), but also in many other environments: in fresh- and brackish-water sediments (Hornibrook and Longstaffe, 1996), in Canadian Arctic desert soils (Kodama and Foscolos, 1981), in coal measures (Iijima and Matsumoto, 1982), in oil sands (Hornibrook and Longstaffe, 1996), and in low-temperature metamorphic and hydrothermally altered rocks (Xu and Veblen, 1996). It is a trioctahedral 1:1 layered silicate having a basal spacing of 7 Å and shows a pleochroic appearance (Brindley, 1982; Bhattacharyya, 1983; Rivas-Sanchez et al., 2006). Berthierine is a mixture of ferrous iron- and magnesium-end members of the serpentine group. Conventional X-ray diffraction (XRD) is limited to differentiating berthierine from other minerals belonging to the chlorite–serpentine group (e.g., Fe-rich chlorite or odinite), because berthierine shares many identical XRD lines with such minerals due to chemically and structurally similarities (Odin, 1990; Rivas-Sanchez et al., 2006). Berthierine formation necessitates reducing conditions in combination with corresponding pH levels and a reasonable chemical composition of aqueous solutions (Bhattacharyya, 1983; Fritz and Toth, 1997). Experimental studies indicate that berthierine formation is restricted to reducing conditions (Sheldon and Retallack, 2002). Newly formed berthierine is unstable in the presence of molecular oxygen, and, subsequently, can be transformed into other minerals depending on the prevailing pH-E_H conditions (Rivard et al., 2013).

The Siri oilfield is located in the Danish North Sea and is a part of the Siri Canyon (Ohm et al., 2006). The present temperature–pressure reservoir conditions of the Siri field are 78 °C and 230 atm (Nice et al., 2000). The investigations performed by

* Corresponding author. Tel.: +49 5323 72 2234; fax: +49 5323 72 2903.
E-mail address: wolfgang.van.berk@tu-clausthal.de (W. van Berk).
[1] Present address: Clausthal University of Technology, Department of Hydrogeology, Leibnizstraße 10, D-38678 Clausthal-Zellerfeld, Germany.

http://dx.doi.org/10.1016/j.marpetgeo.2015.01.007

Stokkendal et al. (2009) and Fu (2014) provided an overview about the reservoir rocks and gave a first insight into the diagenetic processes of the Siri field. Stokkendal et al. (2009) suggested that one of the most important diagenetic processes observed in the Siri field is berthierine formation as a result of the water-wet reservoir rocks in an open system. This open system was considered to be exposed to an advective, long-lasting fluid flow, which steadily delivered aqueous species (e.g., $Fe^{2+/3+}$, Mg^{2+}, H_4SiO_4, and $Al(OH)_x^{+3-x}$ derived from external sources) and admixed them in appropriate stoichiometric ratios for berthierine formation. In general, the total concentrations of these aqueous species ($c_{tot}i_{(aq)}$ for aqueous species i) are controlled by solubility equilibria, and commonly remain at very low levels in aqueous solutions under moderate pH-E_H conditions (e.g., $c_{tot}Al^{3+}_{(aq)}$ of 6.9×10^{-7} mol kgw^{-1} in a 1.0 molal NaCl solution in equilibrium with gibbsite at 78 °C and 230 atm calculated by using the computer code PhreeqcI; Parkhurst and Appelo, 2013). Thus, it seems impossible that externally sourced components could cause the mass conversion of berthierine formation which was observed for the reservoir rocks in the entire Siri field (ca. 5–15 vol.-% according to Stokkendal et al., 2009).

The alteration of the reservoir mineral assemblage in relation to the residual oil in the Siri field was investigated by using various methods: thin section microscopy, scanning electron microscopy (SEM), electron microprobe analysis (EMPA), and high-resolution transmission electron microscopy (HR-TEM). They suggested a close interaction between newly formed minerals and residual oil. Their descriptive results indicate that *in situ* hydrocarbon–water–rock–gas interactions are the driving forces of the diagenetic features. In a first attempt, Fu (2014) performed simple hydrogeochemical batch modeling to investigate berthierine formation in the Siri field. However, this batch modeling only considers a selected part of the complex and interconnected water–rock–gas processes.

Formation of authigenic berthierine in the Siri oilfield exerts a negative influence on the permeability of the reservoir rocks: from ca. 200 mD down to ca. 1 mD with strong berthierine formation (ca. 5–15 vol.-%; Stokkendal et al., 2009). Thus, the present contribution aims (1) to decipher the mechanisms of berthierine formation in the glauconitic oil reservoir, (2) to unravel the parameters which controlled berthierine formation, and (3) to characterize the reservoir units which may be sensitive to berthierine formation and permeability changes. In order to answer these questions in a quantitative way, a complex hydrogeochemical model that is based on thermodynamics of chemical equilibrium was developed. The diagenetic features observed in the Siri field provide a suitable plausibility check of our hydrogeochemical model. The most important diagenetic features in this oil field are briefly reviewed in the following section.

2. Diagenetic features in the Siri field

2.1. Mineralogy

Many studies demonstrate that organic–inorganic interactions trigger significant water–rock–gas reactions in different subsurface environments (e.g., Arning et al., 2011; Schulz and van Berk, 2009; van Berk et al., 2009, 2013). In terms of such organic–inorganic interactions, most hydrocarbon reservoir rocks can be considered to be chemically reactive. Various processes can induce complex reaction chains among minerals, formation water, oil-derived aqueous hydrocarbons, and a multi-component gas, and leave their signatures in form of a new mineral phase assemblage.

Table 1
Diagenetic features of the Siri oilfield.[a]

	Primary particles	Diagenetic features		
		Dissolution	Transformation	Formation
Quartz	x[b]			overgrowth or fine crystals
Glauconite	x	x	to mica[c]	
K-feldspar	x	x		
Albite	x	x		
Muscovite	x			fine crystals
Berthierine				fine crystals or coating
Kaolinite				booklets
Siderite	x			fine crystals
Calcite				crystals or cement
Pyrite				fine crystals

Blanks indicate that the corresponding features were not observed.
[a] Compare Figure 1.
[b] Corresponding diagenetic features were observed.
[c] Via dissolution of glauconite and precipitation of mica.

The reservoir rock matrix of the Siri field is characterized by diagenetic features which are briefly summarized in Table 1 and Figure 1 (for details, see Fu, 2014). One of them is glauconite alteration. Primary glauconite shows various alteration stages: nearly unaltered, partly altered and transformed to mica, significantly altered, and virtually dissolved (Fig. 1a, g, and h). Another Fe-rich mineral that newly formed under reducing conditions in the Siri field was identified as berthierine by combining a series of analytical methods: (1) showing an olive brown color and a pleochroic appearance (thin section microscopy), (2) belonging to the chlorite–serpentine group (conventional XRD), (3) displaying a chlorite-like morphology (SEM; Fig. 1e), (4) identified as a Mg-bearing and Fe-rich silicate (SEM or EMPA), and (5) with a basal spacing of 7 Å in lattice fringes (HR-TEM). Berthierine is characterized by various morphological types: thin coatings, coating nets, elongated and fine crystals (Fig. 1a, b, d, g, and h). It occurs throughout the sandstones: from the gas cap, the oil leg, the OWCs, and down to the water leg, but mainly in the oil leg and at OWCs. Berthierine commonly coats glauconite grains or grows within altered glauconite grains (Fig. 1a, g, and h). This points to the fact that berthierine formation in the Siri field is related to glauconite alteration. In contrast to organic matter-rich, glauconitic environments (e.g., the Nullawarre Greensand; Boyd et al., 2004), berthierine formation and associated glauconite alteration in the Siri field evolved within the reservoir units which are free of sedimentary organic matter.

Carbon dioxide is one of the typical components in petroleum systems and its generation is an inevitable consequence of various processes in view of chemical thermodynamics, such as kerogen maturation, oil generation, and oil degradation (Seewald, 2003; Helgeson et al., 2009). It triggers a series of chemical water–rock–gas reactions in many oil reservoirs, such as feldspar dissolution due to pH buffering (e.g., van Berk et al., 2013). In the Siri field, the feldspar assemblages (K-feldspar and albite; Fig. 1c and d) show dissolution and are free of Ca-bearing plagioclase. By means of hydrogeochemical modeling, van Berk et al. (2009, 2013) demonstrated that carbonic acid-driven dissolution of different feldspars occurs at different pH levels and controls carbon dioxide partial pressures ($pCO_{2(g)}$) prevailing in oil reservoirs. Moreover, these studies reveal that K-feldspar remains stable when anorthite and subsequently albite dissolve. Thus, it seems reasonable to assume that Ca-bearing plagioclase has been initially present in the reservoir rocks of the Siri field (prior to oil charging) and completely dissolved due to interconnected chemical water–rock–gas reactions. Calcium

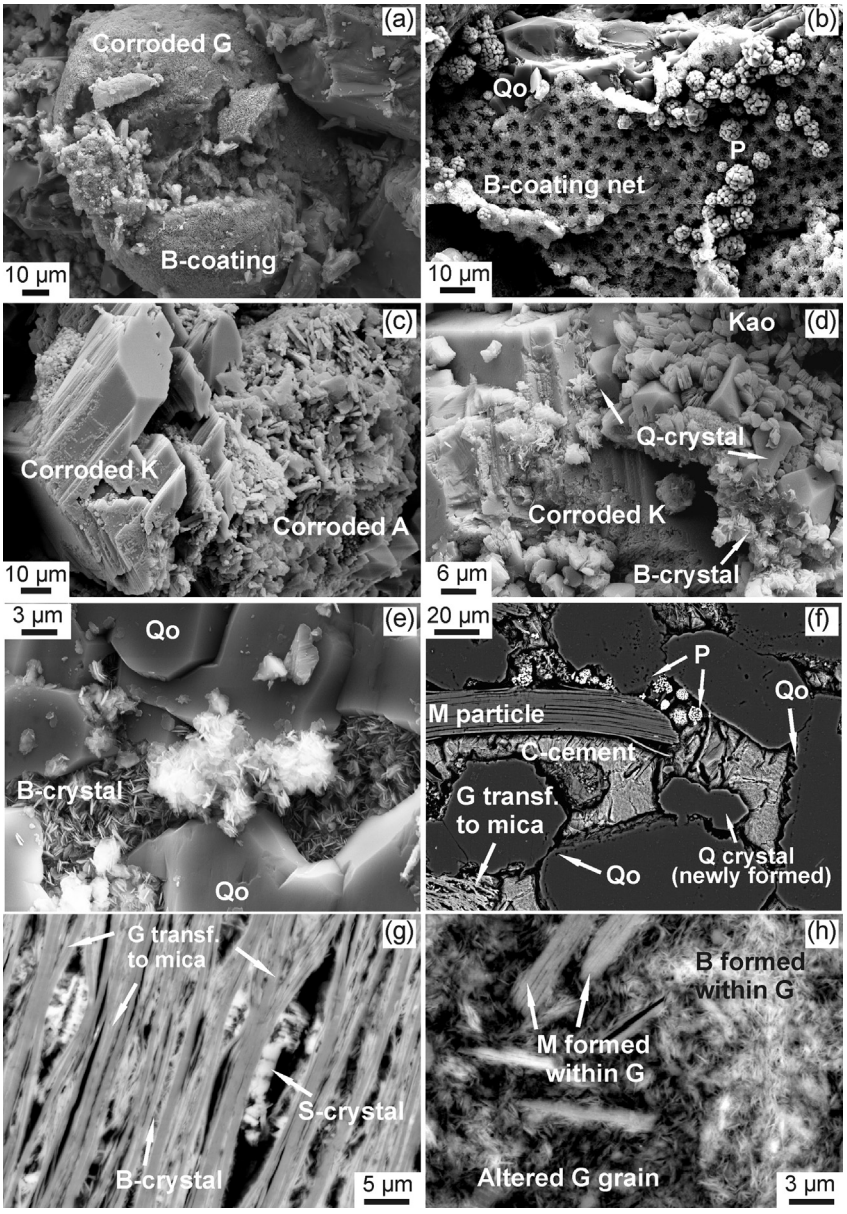

Figure 1. Main diagenetic features observed in the reservoir sandstones of the Siri field. (a) to (e): SEM images; (f): EMPA image with back-scattered detector (BSE); (g) and (h): SEM-BSE images; (a) Corroded glauconite grain coated by berthierine, modified according to Fu (2014); (b) Pyrite on a berthierine net; (c) Corroded K-feldspar and albite; (d) Newly formed kaolinite, quartz, and berthierine on the surface of corroded K-feldspar; (e) Elongated berthierine crystals filling pore space surrounded by quartz overgrowth; (f) Newly formed quartz as small crystals or as overgrowth and calcite cementation at OWC; (g) Fine crystals of siderite and berthierine newly formed between the lamella of mica transformed from the primary glauconite grain; (h) Muscovite and berthierine newly formed within an altered glauconite grain. A: albite; B: berthierine; C: calcite; G: glauconite; K: K-feldspar; Kao: kaolinite; M: muscovite; P: pyrite; Q: quartz; Qo: quartz overgrowth; S: siderite; transf.: transformed.

ions released by anorthite dissolution could react with aqueous $CO_3^{2-}{}_{(aq)}$ species to form calcite. Calcite precipitation in the oil and water legs of the Siri field was proven in only several samples. Massive calcite cement, which completely fills the pore space (Fig. 1f), was observed only at the OWCs and was formed due to the inflow of chalk water driven by seismic pumping (Fu, 2014). This process is excluded from our study. In analogy to calcite, secondary siderite was observed in few core samples (Fig. 1g). Magnesium-bearing carbonates are absent, although the reservoir sandstones are rich in Fe-, Mg-, and carbonate species.

In the Siri field, authigenic quartz occurs as small crystals or overgrowth in all core samples (Fig. 1b, d–f). In addition, formation of some kaolinite took place (Fig. 1d). Muscovite occurs in two distinct forms. Large and intact crystals of muscovite are regarded as primary sedimentary particles (Fig. 1f). Small crystals of muscovite were identified by their microscopic appearance and/or their chemical composition (Fig. 1h), but can also inherit the original color of primary glauconite from which they were transformed (e.g., Fig. 44 in Fu, 2014). Such observations reveal that muscovite was not only present as a primary and sedimentary mineral in the Siri field rocks, but also newly formed due to hydrocarbon–water–rock–gas interactions. Dapples (1967) suggested that muscovite formation preferentially occurs in glauconite-bearing sandstones due to available potassium in the lattice of mica. Therefore, muscovite precipitation in the Siri field is an additional indication of intensive glauconite alteration.

2.2. Oil degradation

In terms of chemical thermodynamics, hydrocarbons are unstable in the presence of water, and are consequently degraded to other components via different pathways (Helgeson et al., 1993; Seewald, 2003; Larter et al., 2006; Jones et al., 2008), even within a closed system (Head et al., 2003). Therefore, the oil–water contact (OWC) can be considered to be a chemically reactive site where oil degradation commonly proceeds via methanogenic hydrocarbon degradation (Head et al., 2003, 2010; Larter et al., 2006; Dolfing et al., 2008; Jones et al., 2008). The oxidation of aqueous *n*-alkanes proceeds via five steps in the presence of water under elevated temperature–pressure conditions, which can be described as hydrolytic disproportionation of aqueous *n*-alkanes (Seewald, 2003). During these steps, aqueous *n*-alkanes are gradually degraded via alkenes, ketones and alcohols, and finally, to methane (CH_4), carbon dioxide (CO_2), hydrogen (H_2) and carboxylic acids (dominantly acetic acid; CH_3COOH; Eqs. (1a) and 1b; Seewald, 2003).

$$R{-}CH_2{-}CH_2{-}CH_{3(n\text{-alkanes})} + 4H_2O \rightarrow R + 2CO_2 + CH_4 + 5H_2 \quad (1a)$$

$$R{-}CH_2{-}CH_2{-}CH_{3(n\text{-alkanes})} + 4H_2O \rightarrow R + 1.9CO_2 + 0.9CH_4 + 0.1CH_3COOH + 5H_2 \quad (1b)$$

Consumption of H_2 produced during *n*-alkane degradation, for instance oxidation of H_2 by ferric iron species, continuously promotes hydrolytic disproportionation of aqueous *n*-alkanes (Meier, 2012). Experiments reveal that ferric iron-bearing minerals could accelerate such an oxidation of *n*-alkanes (Seewald, 2003). The reservoir rocks of the Siri field dominantly consist of quartz and glauconite which is characterized by high ferric iron contents (Amouric and Parron, 1985). The glauconite grains display clear features of alteration which releases ferric iron ions into pore water (Fig. 1). Petrographic investigations demonstrate that ferrous iron-rich berthierine formation is related to glauconite alteration (section 2.1). Due to different oxidation states of iron in the both iron-bearing minerals, this process is dependent on reducing agents in the reservoir rocks of the Siri field which are free of sedimentary organic matter but which are filled by oil. Moreover, newly formed minerals and altered, primary glauconite are closely associated with the residual oil phase (e.g., berthierine precipitated in the residual oil; Fig. 2). The formation water composition in the Siri field shows a high total concentration of organic acids and their anions (ca. 320 mg L^{-1} measured by Nice et al., 2000) which are the typical oil degradation products. On a micrometer scale, the chemical composition of the residual oil phase was investigated by HR-TEM at different sites in a same sample: the oil phase with and without surrounding minerals newly formed (Fu, 2014). This investigation indicates compositional alteration of the residual oil in form of a slight enrichment of sulfur and nitrogen in the oil phase surrounded by the newly formed minerals, when compared to the nearby oil in those regions which lack newly formed minerals.

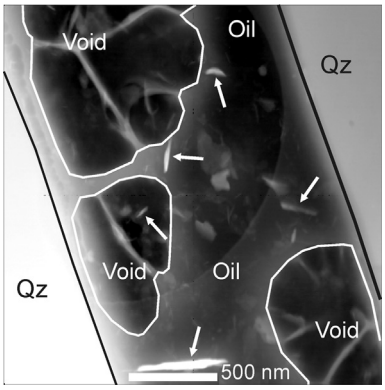

Figure 2. HR-TEM image of authigenic berthierine (white arrows) around and in several voids previously filled by pore water in residual oil (micro-water–oil emulsion) filling the pore space between two quartz grains (Qz; modified according to Fu, 2014).

Oil–water contacts are not restricted *sensu stricto* to the zone between the oil leg and the underlying water leg on a reservoir scale. They can also exist as micro OWCs at the interface between oil phase in rock pores and irreducible pore water films on grain surfaces in water-wet oil reservoirs (Fig. 2), or as the interface between oil phase absorbed on minerals and formation water in the water leg (e.g., Fig. 39 in Fu, 2014). Figure 2 shows that newly formed berthierine is intimately connected to the residual oil phase that fills the pore channel (ca. 1.5 μm wide) between two quartz grains. This oil phase shows a foam-like structure built of residual oil and voids which should have been initially filled by pore water (Fig. 2). Such a foam-like structure could be described as an oil–-water emulsion surrounding the water-wet grains, and consequently, as an OWC on a micrometer scale. Needle-like crystals (50–500 nm in length; Fig. 2) were identified as berthierine due to a basal spacing of 7 Å and to the measured composition (Mg-bearing and Fe-rich aluminosilicate). These crystals seem to float within and around this foam-like structure. Such an OWC phenotype on a micrometer scale is a “hot spot” of intense reactions among aqueous hydrocarbons, aqueous solutions, minerals, and gas.

The oil extracted from the rock samples of the Siri field shows a relative high API grade (Ohm et al., 2006). A regional uplift in the Siri Canyon led to a remigration of hydrocarbons from the Siri field (Ohm et al., 2006). Therefore, the present API is not directly relatable to the present mineral assemblage. In summary, there is a multiple evidence that oil degradation should have occurred and triggered chemical water–rock–gas reactions in the Siri field: (1) a strong alteration of Fe(III)-bearing glauconite potentially reduced by H_2 during *n*-alkane degradation, (2) a high concentration of organic acids measured in the formation water, (3) the compositional alteration of the residual oil observed closed to newly formed minerals, and (4) the close spatial relationship between the observed diagenetic minerals and the altered residual oil.

3. Conceptual modeling approach

Our modeling approach aims to decipher the pathways of the diagenetic processes in the Siri field, and to identify the driving forces behind by means of hydrogeochemical modeling. The zero-dimensional (batch) model simulates closed, isothermal, and isochemical systems which achieve a state of chemical equilibrium among pore water, mineral assemblage and multi-component gas (if the sum of the partial pressures of all gas components exceeds the total pressure). Due to its zero-dimensional character, the modeling approach leaves spatial and temporal aspects unconsidered. The model is based on thermodynamics of chemical equilibrium and on the laws of mass action for solids, as well as for aqueous and for gaseous species involved within the system. This model excludes any kinetic aspects because hydrogeochemical fluid–rock interactions rapidly reach near-equilibrium conditions at reservoir conditions (Fu et al., 2012, 2013).

Oil degradation in the Siri field is indicated by analytical methods. This process is integrated in the presented modeling concept which is conceptually based on irreversible hydrolytic disproportionation (section 2.2). Hydrolytic disproportionation leads to formation of carboxylic acids (dominantly acetic acid) as intermediates, which commonly occur in petroleum reservoirs

independent on temperature (Barth, 1991; Helgeson et al., 1993). Decarboxylation of such carboxylic acids results in the formation of additional CO_2 and CH_4. Assuming that 10% of acetic acid remains at the end of oil degradation, equation (1a) changes to equation (1b).

Our modeling simulates a pore water reactor (PWR) that is directly overlain by the OWC. The PWR is open to the influx of oil degradation products (ODP) from the OWC into the PWR due to diffusion. This process destabilizes the hydrogeochemical equilibrium conditions in the PWR. The acidic and reducing components produced by oil degradation (see Eqs. (1a) and (b)) affect the pH-E_H conditions of the formation water via pH-controlling H^+-transfer reactions and redox-controlling electron-transfer reactions. Such reactions activate the acid and redox buffer capacity of the reservoir mineral assemblage. Dissolution of primary minerals, precipitation of authigenic minerals, and formation of a multi-component gas take place in a complex web of organic–inorganic interactions.

The conceptual batch PWR with a pore volume of 1.0 L is filled with water. It has a temperature of 78 °C and a total pressure of 230 atm similar to the present reservoir condition of the Siri field (Nice et al., 2000). A 1.5 molal NaCl solution (according to the $c_{tot}Cl^-_{(aq)}$ of 56 g L^{-1} measured by Nice et al., 2000) is equilibrated with the primary mineral assemblage (Table 2) in order to calculate the initial pore water composition (prior to oil degradation) in the PWR. A stepwise addition of ODP into the pore water mimics the diffusive transfer of ODP from the OWC to the PWR. Our standard modeling scenario, named as "Siri-ODP" (Table 3), investigates how oil degradation and the thereby triggered hydrogeochemical processes alter the initial reservoir mineral assemblage of the Siri field. Assuming a high porosity of 33% based on petrographic investigations, the PWR has a total volume of 3.0 L, two thirds of which are occupied by a primary mineral assemblage. This mineral assemblage has a total mass of 5.3 kg according to an assumed average grain density of 2.65 kg L^{-1}. Quartz dominates the primary mineral assemblage with ca. 65 wt.-% (Table 2). In the model, the primary quartz grains are only allowed to dissolve. In contrast, chalcedony (cryptocrystalline $SiO_{2(s)}$) is considered as the reactive solid $SiO_{2(s)}$ phase to newly form in the model, because secondary $SiO_{2(s)}$ occurs as individual small crystals or as crystal overgrowths in the Siri field. Glauconite accounts for ca. 20 wt% of the primary mineral assemblage of the reservoir rocks. Petrographic investigations show that glauconite commonly has alteration/dissolution features. As a result, it is assumed that only 30% of the primary glauconite is available for the hydrogeochemical reactions in the PWR (Table 2). Due to the lack of thermodynamic data, the conceptual model replaces feldspar solid solutions by their pure end-members (K-feldspar, albite, and anorthite) prior to the onset of oil degradation (in total 10 wt.-%; Table 2), although no Ca-plagioclase was proven. Moreover, muscovite occurs as a primary mineral (1.0 wt.-% as a rough estimate). The initial pore water in the generic PWR is free of sulfate species and other oxidants. Under anoxic reducing conditions, pyrite can be regarded as a stable, chemically non-reactive mineral, and is therefore excluded from the mineral assemblage.

Dissolution of primary minerals, such as glauconite and feldspar, can buffer the uptake of reducing and acidic ODP. Ferric iron species produced by glauconite dissolution (Eq. (2)) can be reduced to $Fe^{2+}_{(aq)}$ by electron donors (e.g., CH_4 in Eq. (3) or H_2). Such reductive glauconite dissolution increases the aqueous concentrations of Fe^{2+}, Mg^{2+}, Al^{3+}, and H_4SiO_4 which are the major components of berthierine. Consequently, formation of berthierine can be induced at its supersaturation. The average composition of berthierine (Eq. (4)) was measured by EMPA in the Siri field and slightly modified by excluding Ca^{2+}, K^+, and Na^+ which may have been bound in berthierine due to cation exchange.

$$K_{0.489}Na_{0.045}Mg_{0.281}Al_{1.387}Fe_{1.183}Si_{3.327}O_{10}(OH)_{2(Glauconite)} + 10H_2O \leftrightarrow 0.489K^+ + 0.045Na^+ + 0.281Mg^{2+} + 1.387Al(OH)_4^- + 1.069Fe^{3+} + 0.114Fe^{2+} + 3.327H_4SiO_4 + 3.144OH^- \quad (2)$$

$$8Fe^{3+} + CH_{4(aq)} + 2H_2O \rightarrow 8Fe^{2+} + CO_{2(aq)} + 8H^+ \quad (3)$$

$$Fe_{1.634}Mg_{0.328}Al_{1.324}Si_{1.526}O_5(OH)_{4(Berthierine)} + 7.896H^+ \leftrightarrow 1.634Fe^{2+} + 0.328Mg^{2+} + 1.324Al^{3+} + 1.526H_4SiO_4 + 2.896H_2O \quad (4)$$

Moreover, dissolution of glauconite and feldspar can significantly increase $c_{tot}K^+_{(aq)}$, $c_{tot}H_4SiO_{4(aq)}$, and $c_{tot}Al^{3+}_{(aq)}$. This could lead to a supersaturation of the pore water with respect to chalcedony and muscovite, and, consequently, enables their formation. The primary mineral composition of the reservoir rocks in the Siri field is rich in Fe and Mg (in glauconite) and contains trace amounts of Ca (in anorthite). Consistently, siderite, magnesite, dolomite, and calcite may form at saturation. In analogy, other potential secondary minerals that are listed in the used thermodynamic database ("phreeqc.dat"; Parkhurst and Appelo, 2013) are allowed to form,

Table 2
Initial and pre-assigned amounts of the primary and secondary minerals in the PWR for modeling scenario "Siri-ODP".

	Amount[a]	
	wt.-%	mol
Primary minerals		
Quartz[b]	65	57.34
Glauconite[c]	6	0.76
Anorthite	4	0.76
Albite	4	0.81
K-feldspar	2	0.38
Muscovite	1	0.13
Secondary minerals		
Berthierine[d]	0	0
Kaolinite	0	0
Chrysotile	0	0
Chlorite7A[e]	0	0
Chalcedony	0	0
Calcite	0	0
Dolomite	0	0
Magnesite	0	0
Siderite	0	0
$Fe(OH)_{3(a)}$	0	0

[a] Based on thin section microscopy.
[b] Primary quartz can only get dissolved; instead, chalcedony forms as secondary $SiO_{2(s)}$.
[c] 30% of the total primary glauconite is assumed to be available for equilibration.
[d] Or berthierine2, depending on the modeling scenarios.
[e] Chlorite with a basal spacing of 7 Å.

Table 3
Modeling scenarios.

	Primary mineral assemblage	Added reactants	Redox conditions
Siri-ODP	Siri field[a]	CO_2, CH_4, H_2	reducing
Siri-ODP-siderite	Siri field + goethite[b]	CO_2, CH_4, H_2	reducing
Siri-ODP+HAc	Siri field	CO_2, CH_4, H_2, HAc[c]	reducing
Siri-ODP-Be2[d]	Siri field	CO_2, CH_4, H_2	reducing

[a] See Table 2.
[b] The primary mineral assemblage of the Siri oilfield (see Table 2) plus 1 wt.-% goethite.
[c] Acetic Acid.
[d] Be2: berthierine2; composition measured by Stokkendal et al. (2009).

when they achieve saturation, such as chrysotile (the pure-magnesium serpentine), kaolinite, chlorite with a basal spacing of 7 Å (chlorite7A from the "wateq4f.dat"; Parkhurst and Appelo, 2013), and $Fe(OH)_{3(a)}$. Precipitation of such secondary minerals would further adjust the pH-E_H conditions and induce the other reactions within the complex web of hydrogeochemical reactions evolving in the PWR. In other words, the model developed in this study is not calibrated according to any measured or observed data, but is solely based on the principal laws of chemical thermodynamics.

The computer code PhreeqcI (Parkhurst and Appelo, 2013) is our modeling tool. Based on chemical thermodynamics and on the fundamental laws of conservation of mass and charge, PhreeqcI calculates the species distribution of chemical equilibrium among minerals, aqueous solutions, and gases. Its thermodynamic database "phreeqc.dat" (Parkhurst and Appelo, 2013) was used in the model and includes all equilibrium reactions, their corresponding equilibrium constants, and the temperature–pressure dependence of these constants for all involved aqueous, solid and gaseous species except for magnesite, chlorite7A, glauconite, and berthierine (characterized by different chemical compositions). The thermodynamic data of these minerals have been additionally defined in the input file (for details, see Appendix A). Based on the measured chemical composition and the assumed crystal structure of glauconite and berthierine, their thermodynamic properties were calculated by using the predictive approach, which was developed for estimating the thermodynamic properties of phyllosilicates (Vieillard and Mathieu, 2009; Vieillard et al., 2011, and references therein; for details, see Appendix A). PhreeqcI uses the molar volume of minerals to calculate the pressure dependence of the equilibrium constants (Parkhurst and Appelo, 2013). The grain density of glauconite and berthierine depends on their chemical composition, and consequently varies between 2.4 and 2.95 kg L^{-1} (Patchett et al., 1993) and between 3.1 and 3.5 kg L^{-1} (Mandarino and Anderson, 1989), respectively. Assumed values of 2.7 kg L^{-1} and 3.3 kg L^{-1} are used for the density of glauconite and berthierine in our study.

Compared to the standard scenario Siri-ODP, an alternative scenario Siri-ODP+HAc additionally considers production of acetic acid during oil degradation (Table 3). As berthierine is a solid solution consisting of pure ferrous iron- and magnesium-serpentine minerals, its composition slightly varies depending on the pore water composition during growth. However, the hydrogeochemical model is incapable of considering this phenomenon. Therefore, another scenario Siri-ODP-Be2 integrates berthierine with a chemical composition according to Stokkendal et al. (2009; $Fe_{1.738}Mg_{0.417}Al_{0.95}Si_{1.71}O_5(OH)_4$; labeled as "berthierine2"; Table 3) as a potential secondary mineral instead of berthierine with a composition described by equation (4). This scenario shall test the effects of variable berthierine composition on the calculated species distribution.

4. Modeling results

All modeling scenarios start with the primary mineral phase assemblage and allow precipitation of potential secondary minerals at their saturation. The calculated results, including the alteration of the mineral assemblage in the PWR, as well as the modeled pH and E_H, are shown as a function of the reaction steps. The reaction steps are proportional to the amount of added reactants (ODP) and correspondingly represent the intensity of oil degradation. In addition, the increasing amount of the reactants could result in the development of a coexisting gas. The presentation of these parameters aims to identify the mechanisms of the diagenetic features observed in the Siri field.

4.1. Basic scenario "Siri-ODP"

Addition of oil degradation products (ODP) into the PWR induces proton- and electron-transfer reactions which strongly change the pH and E_H conditions. Due to the addition of CH_4 and H_2, the modeled E_H decreases to −580 mV after the first step of ODP addition (Fig. 3a). Under such reducing conditions, Fe^{3+}-ions released by glauconite dissolution are reduced to Fe^{2+}-ions. This leads to an undersaturation with respect to any Fe^{3+}-bearing mineral. With ongoing ODP addition, CO_2, which is produced by oil degradation and additionally via anoxic CH_4 oxidation by Fe^{3+} (Eq. (3)), is continuously released into the pore water. Parallel to this, the modeled pH displays no incrementally decreasing trend as a consequence of ODP addition. The corresponding dissolution of different minerals buffers pH which decreases via three distinct levels: from ca. 10.0, via 9.0, down to 7.0 (Fig. 3a). Strongly reducing conditions evolve in the PWR due to the excess of ODP over the amount of the chemically reactive, available glauconite. Consequently, glauconite completely dissolves at first and buffers the pH due to CO_2 addition into the pore water (Fig. 3b). Then anorthite dissolution takes over the pH buffer from glauconite (Fig. 3c). Dissolution of glauconite and anorthite keeps the pH at an almost constant level of ca. 10 despite intense CO_2 addition during the first four steps. As a result of strong glauconite dissolution, the high $c_{tot}Fe^{2+}{}_{(aq)}$ in combination with the high $c_{tot}Mg^{2+}{}_{(aq)}$ and $c_{tot}H_4SiO_{4(aq)}$ leads to berthierine formation (Fig. 3d). Precipitation of berthierine displaying a very low solubility leads to a very low $c_{tot}Fe$ ($<1 \times 10^{-9}$ mol kgw^{-1} at all reaction steps). Within the first six reaction steps, chrysotile and chlorite7A firstly form (<0.1 wt.-%; Fig. 3f), and subsequently dissolve.

The release of potassium from altered glauconite supports muscovite precipitation. The simultaneous formation of berthierine and muscovite keeps the amount of chalcedony low within the first three reaction steps despite a significant supply of silica species from dissolution of glauconite and anorthite (Fig. 3d). At high pH, added CO_2 is partly converted to CO_3^{2-} species and results in calcite formation which continues at the expense of anorthite (Fig. 3c and e). In spite (1) of a strong glauconite dissolution, (2) of the resulting release of Fe- and Mg-species into the pore water, and (3) of high pCO_2 levels, formation of Fe-bearing carbonates is prevented and only trace amounts of Mg-bearing carbonates form due to the strong Fe- and Mg-fixation via berthierine formation (Fig. 3e). This highlights that the iron ions originally bound in the glauconite lattice are not the source of the observed siderite precipitation (e.g., Fig. 1g).

After dissolution of anorthite, the ongoing dissolution of K-feldspar and albite buffers the CO_2 acidity. Concurrently, precipitation of muscovite and chalcedony continues (Fig. 3d). Kaolinite formation starts with intense dissolution of feldspars and peaks when feldspars completely dissolve (Fig. 3c and d). This reveals that glauconite dissolution is not the control of kaolinite formation observed in the Siri field, although it also releases massive $Al^{3+}{}_{(aq)}$ and $H_4SiO_{4(aq)}$. From the 6th reaction step on, a free gas phase dominated by $CH_{4(g)}$ develops with an increasing content of $CO_{2(g)}$ (Fig. 3b).

4.2. Further scenarios

The calculated results of scenario Siri-ODP show that dissolution of Fe-rich glauconite is not the reason of the siderite formation observed in the Siri field. Thus, an alternative modeling scenario (Siri-ODP-siderite) considers goethite (FeOOH) as a further primary mineral, which is one of the most common products of oxic glauconite weathering (Longuépée and Cousineau, 2006). It was assumed that 1.0 wt.-% of goethite additionally exists in the primary

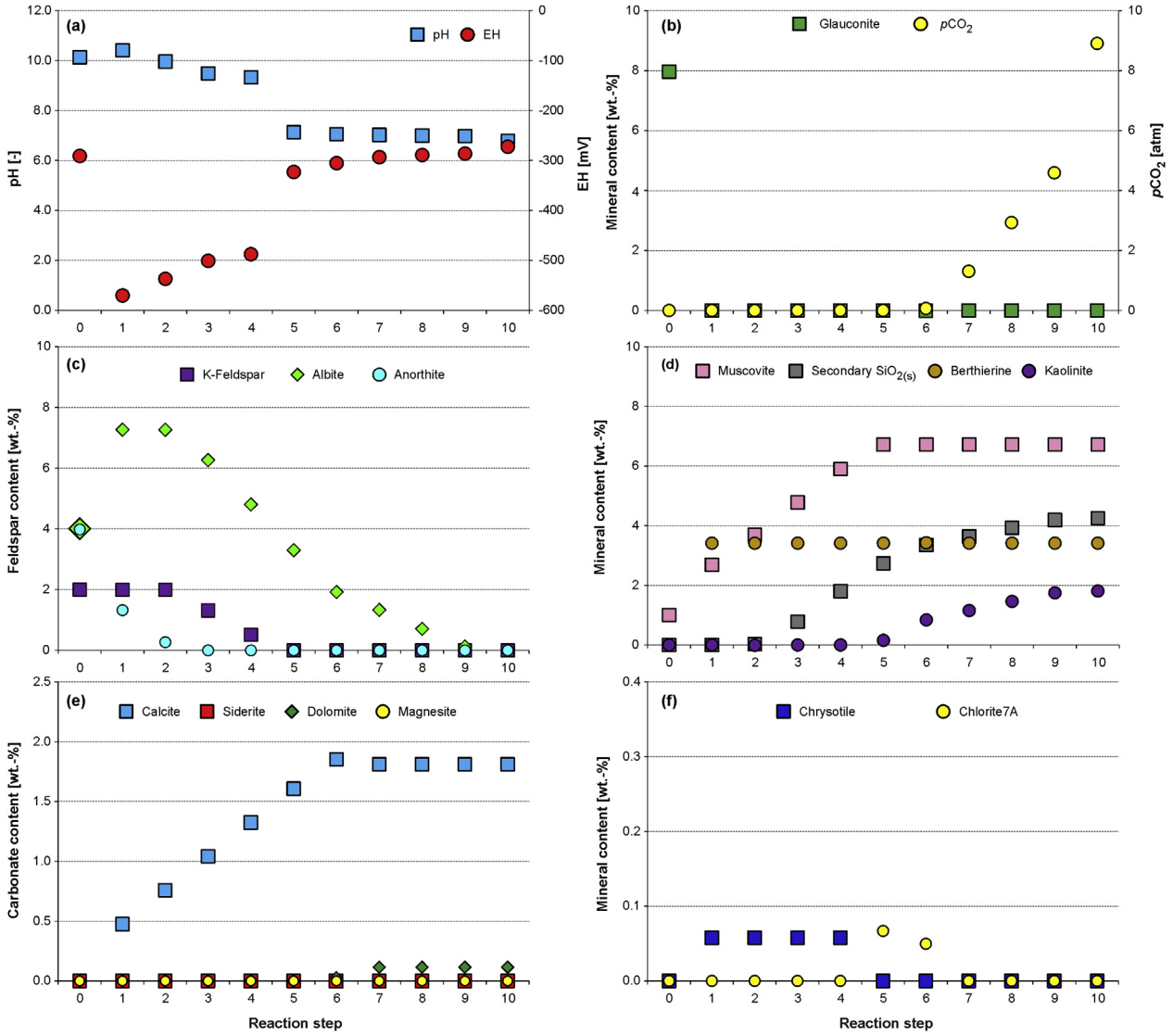

Figure 3. Results of modeling scenario Siri-ODP which simulates an increasing addition of oil degradation products into pore water (reaction steps 1–10). Amount of reactants incrementally added: 0.2 mol CH_4, 0.4 mol CO_2, and 1.0 mol H_2 per reaction step.

mineral assemblage of scenario Siri-ODP-siderite prior to oil degradation (compared to scenario Siri-ODP). The modeling results show that the high pH caused by dissolution of glauconite and feldspar prevents strong goethite dissolution during the first seven reaction steps despite strongly reducing conditions (Fig. B.1a–c and f). Parallel to this, siderite precipitation starts at the 8th reactions step, as the primary glauconite and feldspar completely dissolve (Fig. B.1b, c, and e). At the final reaction step, 0.9 wt.-% siderite forms at the expense of goethite (Fig. B.1e–f). Siderite formation additionally extracts carbonate species from the aqueous solution, and, consequently, $pCO_{2(g)}$ decreases (Fig. B.1b). The other parameters including the amount of newly formed berthierine still show identical trends and also similar absolute levels when compared to scenario Siri-ODP (Figs. 3a–f and B.1a–f).

In scenario Siri-ODP-Be2, berthierine2 (composition according to Stokkendal et al., 2009) is slightly enriched in Fe but impoverished in Mg compared to berthierine in scenario Siri-ODP. The total amount of carbonates in scenario Siri-ODP-Be2 decreases and the calculated pCO_2 slightly increases at the same reaction step as in the Siri-ODP scenario (Figs. B.2b–c and 3b–c). Due to the distinct Al:Si ratios in berthierine, the amounts of Al- and/or Si-bearing minerals slightly vary in these two scenarios (Figs. 3c–d and B.2c–d). The results of the further scenario (Siri-ODP+HAc), which is extended by further addition of acetic acid, resemble those of scenario Siri-ODP with regard to all parameters (Figs. 3a–f and B.3a–f).

5. Discussion and implications

The modeled alteration of the reservoir mineral assemblages in the Siri field fits the results gained by various analytical methods (section 2), showing (1) berthierine formation at the expense of glauconite, (2) depletion of K-feldspar and albite coupled to formation of kaolinite and secondary $SiO_{2(s)}$, (3) moderate precipitation of muscovite, and (4) prevention of Fe- or Mg-carbonate precipitation despite enrichment of Fe-, Mg-, and carbonate species in this field. Our modeling demonstrates that hydrocarbon–water–rock–gas interactions are the driving force of these diagenetic processes, which is supported by the observed close relationship between the diagenetic minerals and the altered

residual oil. The calculated results and the observations indicate weak calcite formation in the reservoir. Ca-bearing plagioclase has not been detected in the reservoir rocks, whereas its dissolution results in calcite formation in the modeling. This might suggest that Ca-bearing plagioclase dissolved in the reservoir. A modeled low-degree oil degradation leads to high pH which in combination with the high sodium concentration of the formation water causes weak albitization (Fig. 3c). However, albitization was not observed in the analyzed samples. This difference points to the fact that the present reservoir rocks of the Siri field may have undergone weak oil degradation. The modeling results show that pure-Mg serpentine and chlorite with minor amounts (chrysotile and chlorite7A) could form depending on the oil degradation intensity. However, no pure-Mg silicate was proven. This indicates that "fresh" berthierine may have a variable composition due to a changing chemical composition of the pore water and can be enriched in Mg at specific stages of glauconite dissolution. However, this change in the chemical composition of berthierine is incapable of being included in the model. Despite minor differences, the alteration of the reservoir rocks, which is calculated based on thermodynamics of chemical equilibrium, well match the observations of the reservoir mineral assemblages. Hence, this good accordance confirms the plausibility of the developed hydrogeochemical model.

Our modeling results reveal that strong alteration of Fe-rich glauconite is not a control of siderite precipitation. Actually, siderite newly forms, as primary glauconite and feldspar completely dissolve and goethite begins to dissolve. Therefore, dissolution of iron(III) oxide–hydroxide (e.g., goethite), which commonly occurs as one of the weathering products of glauconite, may have resulted in noticeable siderite formation in the Siri field. Micro-environments, which contain iron(III) oxide–hydroxide but which are free of reactive glauconite and feldspar (due to their complete consumption or passivation by coating), may be the favored sites for siderite precipitation. These complex hydrocarbon–water–rock–gas interactions evolve as isochemical, *in situ* transformations (among different components), and are triggered by oil degradation. Additionally, our modeling results indicate that the following two processes exert no influence on the type of diagenetic processes, and slightly control the mass conversion of these diagenetic processes: (1) variation in berthierine composition depending on compositional changes of pore water, and (2) formation of carboxylic acids during oil degradation.

Stokkendal et al. (2009) showed that berthierine formation in the Siri field reduces the reservoir permeability. Additionally, they suggested that berthierine formation resulted from an advective, long-lasting fluid flow which durably delivered aqueous species. If so, berthierine formation should be restricted to narrow areas of the reservoir which are exposed to this fluid flow. In contrast, our modeling unravels that berthierine formed within a more or less closed system. Reducing agents (CH_4 and H_2) produced by oil degradation are the driving forces of glauconite dissolution via reduction of $Fe^{3+}_{(aq)}$ species to $Fe^{2+}_{(aq)}$ species. This reveals that berthierine formation is an inevitable process evolving in the Siri field. Within water-wet glauconitic rocks, berthierine formation thus should be intensified in oil legs and at OWCs which are the "hot spots" of organic–inorganic interactions due to a sufficient supply with reducing agents. This finding matches the main occurrence of secondary berthierine observed in the oil leg and at the OWC in the Siri field. Correspondingly, the changes in reservoir porosity–permeability properties triggered by oil degradation and glauconite dissolution would be focused in the oil leg and at the OWC compared to the water leg. Berthierine formation in the Siri field is a result of the redox-reactions between glauconite and oil degradation products (CH_4 and H_2). Thus, the mass conversion of newly formed berthierine can be used to estimate the amount of degraded oil, because the reservoir sandstones of the Siri field are free of other reducing agents, such as sedimentary organic matter.

Mineral dissolution and precipitation can change porosity and also permeability. Calculating an overall volumetric balance of the total mineral assemblage indicates whether diagenetic processes create secondary porosity or reduce primary porosity. For instance, the calculated total volume of newly formed minerals (including berthierine, calcite, siderite, kaolinite, chalcedony, and muscovite) overcompensates for the summed volume of dissolved primary minerals (glauconite, feldspar, and goethite) in scenario Siri-ODP-siderite (Table 4). At the last reaction step of this scenario, the porosity of the PWR is decreased by ca. 0.47% (14 ml per 3.0 L of the total rock volume; Table 4). Porosity would further decrease, provided that the coupled mineral dissolution and precipitation would continue in glauconite-bearing and berthierine-forming systems. In general, a slight decrease in porosity could lead to a strong permeability reduction due to mineral precipitation (Vaughan, 1987). Hydrocarbon–water–rock–gas interactions are thus the basic control of porosity reduction caused by berthierine precipitation in the Siri field. Thus, it can be deduced that a stronger decrease in reservoir porosity and/or permeability due to glauconite dissolution and the resulting berthierine formation could preferentially proceed in the oil leg and at the OWC compared to the water leg. In summary, the good agreement between the modeled and observed alteration of the reservoir rocks in the Siri field provides a good example for applying hydrogeochemical modeling as a useful tool in order to identify the mechanisms,

Table 4
Calculated volume conversion (in ml) of minerals involved within the PWR (1.0 L pore space; reaction steps 1–10) for scenario Siri-ODP-siderite.

	1	2	3	4	5	6	7	8	9	10
Anorthite	45	64	77	77	77	77	77	77	77	77
Albite	−58	−56	−43	−13	16	47	65	70	71	71
K-Feldspar	0	0	2	19	35	41	41	41	41	41
Calcite	−10	−16	−21	−27	−32	−38	−39	−39	−39	−39
Kaolinite	0	0	0	0	0	−8	−16	−19	−19	−20
Siderite	0	0	0	0	0	0	0	−3	−8	−13
Chalcedony	−6	−7	−15	−35	−55	−72	−81	−82	−82	−83
Glauconite	118	118	118	118	118	118	118	118	118	118
Berthierine	−64	−64	−64	−64	−64	−64	−64	−64	−64	−64
Muscovite	−25	−45	−64	−85	−106	−115	−115	−115	−115	−115
Goethite	4	4	4	4	4	4	4	5	8	12
Sum	3	−2	−6	−6	−7	−10	−10	−11	−12	−14

Negative value (−): decrease in pore volume due to mineral formation; positive value (+): increase in pore volume due to mineral dissolution; ρ: mineral density in kg L^{-1}; ρ(anorthite): 2.76; ρ(anorthite): 2.615; ρ(K-feldspar): 2.563; ρ(calcite): 2.711; ρ(kaolinite): 2.63; ρ(siderite): 3.932; ρ(chalcedony): equals to ρ(quartz) of 2.65; ρ(muscovite): 2.83; ρ(goethite): 4.18; all the mineral densities: taken from mindat.org (2014).

controlling factors, and preferential locations of diagenetic processes and thereby triggered porosity–permeability changes in petroleum systems.

6. Conclusions

Previous hypotheses suggested that berthierine precipitation in the Siri field should have evolved in an open system (Stokkendal et al., 2009). In contrast, a good match between the measured and modeled mineralogical alteration of the reservoir rocks in the Siri field reveals that strong berthierine formation should have resulted from *in situ* glauconite alteration in a more or less closed aqueous system due to hydrocarbon–water–rock–gas interactions. All components necessary to form berthierine can be from internal sources in glauconitic subsurface environments that need to be rich in electron donors, such as the glauconitic reservoir rocks of the Siri field after oil degradation. In glauconitic oil reservoirs, berthierine formation therefore should be more commonly observed in the oil leg and at the OWC where permeability decreases. Moreover, the modeling results highlight that glauconite dissolution and berthierine formation are commonly accompanied by precipitation of potassium mica and $SiO_{2(s)}$. In spite of the strong release of aqueous aluminum and silica species due to glauconite dissolution, kaolinite precipitation observed in the Siri field resulted from feldspar alteration. Although glauconite is characterized by very high iron contents, its dissolution would not lead to siderite precipitation. For this, dissolution of other iron-bearing minerals, such as iron(III)-oxide–hydroxide, may be responsible. Calculations of an overall volumetric balance of the total mineral assemblage indicate that these diagenetic processes triggered by hydrocarbon–water–rock–gas interactions in the Siri field could lead to a reduction in porosity and permeability, mainly in the oil leg and at the OWC.

Acknowledgments

We thank DONG Energy and Niels H. Schovsbo (Geological Survey of Denmark and Greenland, GEUS) who enabled sampling and access to data of the Siri field. We are very grateful to Philippe Vieillard (University of Poitiers) for helping to calculate the thermodynamic properties of clay minerals. Two anonymous reviewers and the associate editor Wolfgang Kalkreuth are acknowledged for their comments that helped to substantially improve the manuscript.

Appendix A. Supplementary data

Supplementary data related to this article can be found at http://dx.doi.org/10.1016/j.marpetgeo.2015.01.007.

References

Amouric, M., Parron, C., 1985. Structure and growth mechanism of glauconite as seen by high resolution transmission electron microscopy. Clays Clay Miner. 33, 473–482.
Arning, E.T., Fu, Y., van Berk, W., Schulz, H.-M., 2011. Organic carbon remineralization and solid-aqueous solution gas interactions: case study ODP Leg 204, Site 1246 (Hydrate Ridge). Mar. Chem. 126, 120–131.
Barth, T., 1991. Organic acids and inorganic ions in waters from petroleum reservoirs, Norwegian continental shelf: a multivariate statistical analysis and comparison with American reservoir formation waters. Appl. Geochem. 6, 1–15.
Bhattacharyya, D.P., 1983. Origin of berthierine in ironstones. Clays Clay Miner. 31, 173–192.
Boyd, G.A., Wallace, M.W., Holdgate, G.R., Gallagher, S.J., 2004. Marine clays and porosity evolution in the Nullawarre Greensand, Otway Basin, southeastern Australia. In: PESA Eastern Australasian Basins Symposium II Held in Adelaide, 20-22 September, 2004.
Brindley, G.W., 1982. Chemical compositions of berthierines–a review. Clays Clay Miner. 30, 153–155.
Dapples, E.C., 1967. Diagenesis of sandstones. In: Larsen, G., Chilingar, G.V. (Eds.), Diagenesis in Sediments. Elsevier, Amsterdam, pp. 91–126.
Dolfing, J., Larter, S.R., Head, I.M., 2008. Thermodynamic constraints on methanogenic crude oil biodegradation. ISME J. (Multidiscip. J. Microb. Ecol.) 2, 442–452.
Fritz, S.J., Toth, T.A., 1997. An Fe-berthierine from a Cretaceous laterite: part II. Estimation of Eh, pH and pCO_2 conditions of formation. Clays Clay Miner. 45, 580–586.
Fu, Y., van Berk, W., Schulz, H.-M., 2012. Hydrogeochemical modelling of fluid–rock interactions triggered by seawater injection into oil reservoirs: case study Miller field (UK North Sea). Appl. Geochem. 27, 1266–1277.
Fu, Y., van Berk, W., Schulz, H.-M., 2013. Temporal and spatial development of scale formation: one-dimensional hydrogeochemical transport modeling. J. Pet. Sci. Eng. 112, 273–283.
Fu, Y., 2014. Development and Application of Numerical Modeling for Evaluating and Predicting Hydrogeochemical Processes Temporally and Spatially Evolving in Petroleum Reservoirs: Case Studies: Miller Oilfield (UK North Sea) and Siri Oilfield (Danish North Sea) (Ph.D. thesis). Clausthal University of Technology, Germany, pp. 71–134.
Head, I.M., Jones, D.M., Larter, S.R., 2003. Biological activity in the deep subsurface and the origin of heavy oil. Nature 426, 344–352.
Head, I.M., Larter, S.R., Gray, N.D., Sherry, A., Adams, J.J., Aitken, C.M., Jones, D.M., Rowan, A.K., Huang, H., Röling, W.F.M., 2010. Hydrocarbon degradation in petroleum reservoirs. In: Kenneth, N., Timmis, E. (Eds.), Handbook of Hydrocarbon and Lipid Microbiology Part 28. Springer-Verlag, Heidelberg, Germany, pp. 3097–3109.
Helgeson, H.C., Knox, A.M., Owens, C.E., Shock, E.L., 1993. Petroleum, oil field waters, and authigenic mineral assemblages: are they in metastable equilibrium in hydrocarbon reservoirs? Geochim. Cosmochim. Acta 57, 3295–3339.
Helgeson, H.C., Richard, L., McKenzie, W.F., Norton, D.L., Schmitt, A., 2009. A chemical and thermodynamic model of oil generation in hydrocarbon source rocks. Geochim. Cosmochim. Acta 73, 594–695.
Hornibrook, E.R.C., Longstaffe, F.J., 1996. Berthierine from the Lower Cretaceous Clearwater formation, Alberta, Canada. Clays Clay Miner. 44, 1–21.
Iijima, A., Matsumoto, R., 1982. Berthierine and chamosite in coal measures of Japan. Clays Clay Miner. 30, 264–274.
Jones, D.M., Head, I.M., Gray, N.D., Adams, J.J., Rowan, A.K., Aitken, C.M., Bennett, B., Huang, H., Brown, A., Bowler, B.F., Oldenburg, T., Erdmann, M., Larter, S.R., 2008. Crude-oil biodegradation via methanogenesis in subsurface petroleum reservoirs. Nature 451, 176–180.
Kodama, H., Foscolos, A.E., 1981. Occurrence of berthierine in Canadian Arctic desert soils. Can. Mineral. 19, 279–283.
Larter, S., Huang, H., Adams, J., Bennett, B., Jokanola, O., Oldenburg, T., Jones, M., Head, I., Riediger, C., Fowler, M., 2006. The controls on the composition of biodegraded oils in the deep subsurface: part II. Geological controls on subsurface biodegradation fluxes and constraints on reservoir fluid property prediction. AAPG Bull. 90, 921–938.
Longuépée, H., Cousineau, P.A., 2006. Constraints on the genesis of ferrian illite and aluminum-rich glauconite: potential impact on sedimentology and isotopic studies. Can. Mineral. 44, 967–980.
Meier, A., 2012. Experimentelle Untersuchungen zu Reaktionen von Erdölverbindungen (n-Alkanen) mit Hämatit-Kutanen in klastischen Erdölspeichergesteinen (Ph.D. thesis). Friedrich Schiller University Jena, Germany (in German), 14 p.
Mandarino, J.A., Anderson, V., 1989. Monteregian Treasures: the Minerals of Mont Saint-Hilaire, Quebec. Cambridge University Press, New York, p. 184.
mindat.org, 2014. The Mineral and Locality Database. http://www.mindat.org (accessed 23.05.14.).
Nice, P.I., Takabe, H., Ueda, M., 2000. The Development and Implementation of a New Alloyed Steel for Oil and Gas Production Wells. NACE International, presented at CORROSION 2000 held in Orlando, 26-31 March, 2000.
Odin, G.S., 1990. Clay mineral formation at the continent-ocean boundary: the Verdine facies. Clay Miner. 25, 477–483.
Ohm, S.E., Karlsen, D.A., Roberts, A., Johannessen, E., Høiland, O., 2006. The Paleocene sandy Siri Fairway: an efficient "pipeline" draining the prolific Central Graben? J. Pet. Geol. 29, 53–82.
Parkhurst, D.L., Appelo, C.A.J., 2013. Description of input and examples for PHREEQC Version 3–a computer program for speciation, batch-reaction, one-dimensional transport, and inverse geochemical calculations. U.S. Geological Survey Techniques and Methods book 6, (Chapter A43), Available only at: http://pubs.usgs.gov/tm/06/a43/.
Patchett, J.G., Wiley, R., Mostafa, E.B., 1993. Modeling the effects of glauconite on some openhole Logs from the Lower Senonian in Egypt. In: SPWLA 34th Annual Logging Symposium, 13-16 June, 1993, Calgary, Alberta. Society of Petrophysicists and Well-log Analysts.
Rivard, C., Pelletier, M., Michau, N., Razafitianamaharavo, A., Bihannic, I., Abdelmoula, M., Ghanbaja, J., Villiéras, F., 2013. Berthierine-like mineral formation and stability during the interaction of kaolinite with metallic iron at 90 °C under anoxic and oxic conditions. Am. Mineral. 98, 163–180.
Rivas-Sanchez, M.L., Alva-Valdivia, L.M., Arenas-Alatorre, J., Urrutia-Fucugauchi, M., Ruiz-Sandoval, M., Ramos-Molina, M.A., 2006. Berthierine and chamosite hydrothermal: genetic guides in the Pena Colorada magnetite-bearing ore deposit, Mexico. Earth Planets Space 58, 1389–1400.
Schulz, H.-M., van Berk, W., 2009. Bacterial methane in the Atzbach-Schwanenstadt gas field (upper Austrian Molasse Basin): part II. Retracing gas generation and filling history by mass balancing of organic carbon conversion applying hydrogeochemical modeling. Mar. Pet. Geol. 26, 1180–1189.

Seewald, J.S., 2003. Organic-inorganic interactions in petroleum producing sedimentary basins. Nature 426, 327–333.
Sheldon, N.D., Retallack, G.J., 2002. Low oxygen levels in earliest Triassic soils. Geology 30, 919–922.
Stokkendal, J., Friis, H., Svendsen, J.B., Poulsen, M.L.K., Hamberg, L., 2009. Predictive permeability variations in a Hermod sand reservoir, Stine Segments, Siri Field, Danish North Sea. Mar. Pet. Geol. 26, 397–415.
van Berk, W., Schulz, H.-M., Fu, Y., 2009. Hydrogeochemical modelling of CO_2 equilibria and mass transfer induced by organic–inorganic interactions in siliciclastic petroleum reservoirs. Geofluids 9, 253–262.
van Berk, W., Schulz, H.-.M., Fu, Y., 2013. Controls on CO_2 fate and behavior in the Gullfaks oilfield (Norway): how hydrogeochemical modeling can help decipher organic-inorganic interactions. AAPG Bull. 97, 2233–2255.
Vaughan, P.J., 1987. Analysis of permeability reduction flow of heated, aqueous fluid through Westerly Granite. In: Tsang, C.F. (Ed.), Coupled Processes Associated with Nuclear Waste Repositories. Academic Press, New York, pp. 529–539.
Vieillard, P., Mathieu, R., 2009. A predictive model for the enthalpies of hydration of zeolites. Am. Mineral. 94, 565–577.
Vieillard, P., Blanc, P., Fialips, C.I., Gailhanou, H., Gaboreau, S., 2011. Hydration thermodynamics of the SWy-1 montmorillonite saturated with alkali and alkaline-earth cations: a predictive model. Geochim. Cosmochim. Acta 75, 5664–5685.
Xu, H., Veblen, D.R., 1996. Interstratification and other reaction microstructures in the chlorite-berthierine series. Contrib. Mineral. Petrol. 124, 291–301. Springer-Verlag.